NANO · MICRO small
www.small-journal.com

Bending-Insensitive Intrinsically Flexible Ultraviolet Encoding Devices Based on Piezoelectric Nanogenerator-Supplied Liquid Crystalline Polymer Fabrics

*Xiaoxiong Zheng, Zhefeng Liu, Rui Wang, and Aihua Chen**

It is significantly challenging for state-of-the-art wearable electronics to stably monitor physicochemical signals under dynamic motions. Herein, a bending-insensitive, self-powered, and intrinsically flexible UV detector has been realized based on well-designed oriented composite fabrics, consisting of ionic liquid (IL)-containing liquid crystalline polymers (ILCPs) and piezoelectric poly(vinylidene fluoride-trifluoroethylene) [P(VDF-TrFE)] nanogenerators. The novel composite fabrics establish effective UV illuminance-internal stress-electric signal conversion by coupling resistive and piezoelectric effects, with a fast response time of 190 ms. Particularly, benefiting from the intrinsic flexibility of composite fabrics, the ILCP/P(VDF-TrFE) device can maintain stable performance under dynamic bending even if the frequency is up to 2.5 Hz, with a bending insensitivity of less than 1% performance variation under 1.0 mW cm^{-2} UV light. Combined with the Internet of Things and the American Standard Code for Information Interchange (ASCII), wearable encoding electronics have been successfully implemented with a printing speed of 3.2 s per character under dynamic bending.

1. Introduction

With the growing reliance on mobile devices and the development of the Internet of Things (IoTs), wearable electronics that can be integrated into human skin or textiles are highly desirable for artificial intelligence, human-machine interfaces, soft robotics, and health monitoring, etc.[1] Among them, Ultraviolet (UV) detectors are attracting worldwide attention recently owing to their broad applications including UV communication, biological and chemical analysis, industrial production, remote control, and memory storage.[2] Particularly, UV communication is essential for military applications in radio-silent condition, benefiting from its intrinsic advantages of anti-interference and anti-interception in short range.[3] To fabricate wearable UV detectors, previous works generally adopted a hybrid approach of integrating rigid photoelectric semiconductors (e.g., titanium dioxide) onto flexible polymer substrates by geometrical designs, featuring excellent sensitivity.[4] In terms of usage requirements under various extreme environments in the military field, the wearable UV detectors integrated into military equipment inevitably suffer from dynamic bending, folding, or vibrating. However, it is still a significant challenge for wearable electronics working under dynamic motions, due to the large mismatch of elastic modulus between rigid semiconductors and flexible polymers, resulting in localized stress at rigid-soft interfaces and interconnect failure.[5] To date, the reported works of wearable electronics, as well as UV detectors, rarely demonstrated stable detecting performance under static bending tests.[6] To meet the growing demand for wearable electronics, it is greatly urgent for dynamically-workable UV detectors to guarantee communication stability.

To address the limitations, recent breakthroughs concentrate on the development of polymer-based sensitive elements for intrinsically flexible electronic devices, offering significant advantages of mechanical robustness, conformability, adhesion, and self-healing.[7] Smart polymers or stimuli-responsive polymers can induce physicochemical property changes, such as shape, color, and conductivity, upon subtle variation in the environment.[8] However, reported photoisomerizable moiety-containing smart polymers for UV detectors seriously suffered from slow response time of several minutes, because the photoisomerizable moieties were simply grafted onto polymer side chains or mixed in the polymer matrix.[9] Liquid crystalline elastomers (LCEs), or crosslinked liquid crystalline polymers (CLCPs), are promising candidates to construct sensitive wearable electronics, featuring robust mechanical properties, lightweight, and fast response to environmental stimuli, due to the synergistic effect of liquid crystalline (LC) alignment and polymer networks.[10] For instance, Jennifer A. Lewis and coworkers demonstrated the innervated LCE actuators composed of liquid metal core and LCE shell via core-shell 3D printing, with programable contractile actuation, self-sensing, and closed loop control.[11] The incorporation of azobenzene

X. Zheng, Z. Liu, R. Wang, A. Chen
School of Materials Science and Engineering
Beihang University
No. 37 Xueyuan Road, Haidian District, Beijing 100191, P. R. China
E-mail: chenaihua@buaa.edu.cn
X. Zheng, Z. Liu, R. Wang, A. Chen
Beijing Advanced Innovation Centre for Biomedical Engineering
Beihang University
No. 37 Xueyuan Road, Haidian District, Beijing 100191, P. R. China
The ORCID identification number(s) for the author(s) of this article can be found under https://doi.org/10.1002/smll.202202639.

DOI: 10.1002/smll.202202639

(Azo) mesogens into LC networks can realize the light-response of CLCPs. Based on the *trans-cis* isomerization of Azo mesogens upon alternative UV and visible light/heating, the Azo-CLCPs undergo a reversible phase transition between an LC anisotropic phase and an isotropic phase, which generates heterogeneous contraction stress and thus reversible macroscopical deformation.[12] Integrated with conductive fills, such as liquid metal and ionic liquids (ILs), by elaborate structural designing, it is potential to rapidly transform the UV-induced stress into electric signals. However, reported works mainly concentrated on the macroscopical deformation of CLCPs.[13] Additionally, it is reported that the sensor performance can be significantly improved via geometric microengineering of the responsive layers, such as microdomes, micropyramids, and microlines/microridges.[14] The reason is that the introduction of air voids between the microstructures facilitates the microscopic deformation of the responsive layers upon external stimuli.[15] We previously demonstrated a robust UV monitoring and shielding device based on Azo-CLCP, IL, and thermoplastic polyurethanes (TPU) composite fabrics with microlines of ≈2.0 μm in diameter by electrospinning.[16] The elastic TPU matrix can transfer the UV light-triggered stress to ILs and then accelerate ion migration, converting to resistive signals rapidly. However, the device exhibits a response time of 5 s, a recovery time of 4 s, and an illuminance resolution of 5 mW cm^{-2}, which is hard to compete with semiconductor-based UV detectors.[4] Combining with the 8-bit encoding of the American Standard Code for Information Interchange (ASCII), the printing speed of the device is ≈72 s per character, which cannot meet the requirement for the complex information communication. The device is a kind of resistive sensor, which tends to suffer from low sensitivity and slow response/recovery speeds, due to the viscoelasticity of matrix.[17] Therefore, the elaborate selection of polymer composites and design of device structures are highly desired for wearable UV detectors with enhanced performance.

Nanogenerators (NGs), that can convert mechanical energy from the environment and human motions into electrical energy, have been widely utilized to power various kinds of sensors for constructing self-powered nanodevices or nanosystems.[18] Representative piezoelectric polymers for NGs are poly(vinylidene fluoride) (PVDF) and its copolymer poly(vinylidene fluoride-trifluoroethylene) [P(VDF-TrFE)], which can be seamlessly integrated into intrinsically flexible textiles or fabrics.[19] The piezoelectric polymer-based NGs can take the place of the external power supply to drive electric signals spontaneously. Compared to the aforementioned resistive effects, the piezoelectric effects generally exhibit higher sensitivity and faster response speed.[20] Additionally, it is reported that the orientation of fibers can further enhance the performance of detectors, due to the improved alignment of dipoles.[21]

Herein, we demonstrate well-defined piezoelectric P(VDF-TrFE) nanogenerator-supplied ionic liquid (IL)-containing liquid crystalline polymer (ILCP) composite fabrics, for bending-insensitive and self-powered wearable UV detectors (**Figure 1**a). Due to the intrinsic flexibility of composite fabrics, the dynamic motions have limited effects on the sensing signals of UV detectors, even under bending frequency of 2.5 Hz with 200 m^{-1} curvatures, with a bending insensitivity of less than 1% performance variation under 1.0 mW cm^{-2} UV light. Owing to their solution-processabilities and compatibility of two polymers, the LCP and P(VDF-TrFE) mixtures are fabricated into fabrics with oriented microlines upon high-speed rotated collector by electrospinning (Figure 1b). Benefiting from the synergistic effects of Azo-LC alignment and polymer networks, the combination of Azo-CLCPs, ILs, and P(VDF-TrFE) establishes an efficient conversion of UV illuminance-internal stress-current signals by coupling of piezoelectric and resistive effects, which substantially facilitates the sensitivity of UV detectors (Figure 1c). The ILCP/P(VDF-TrFE) device demonstrates a highly enhanced response time of 190 ms in the absence of external power supply. Based on it, we have designed the wearable and bending-insensitive on-demand ASCII encoding electronics for UV communication via the Internet of Things technologies, with a printing speed of 3.2 s per character, especially under dynamic bending. The elaborately designed polymer composites and signal conversion mechanism significantly enhance the sensitivity of detectors, and workability under dynamic state, further generating potential applications of wearable electronics in the military and fieldworks.

2. Results and Discussion

2.1. Fabrication of the ILCP/P(VDF-TrFE) Device

In the fabrication process, first, the oriented LCP/P(VDF-TrFE) fabrics were obtained by electrospinning a mixture solution of Azo-LCPs and P(VDF-TrFE) onto a drum collector (wrapped by conductive fabrics) upon high-speed rotation. The Azo-LCPs used in this study are amphiphilic block copolymers, containing 11 wt.% hydrophilic PEO blocks, which have great compatibility with P(VDF-TrFE) (Figure 1d and Figure S1, Supporting Information). Compared with PVDF, the P(VDF-TrFE) copolymers with appropriate TrFE content can easily crystallize in the β-phase structure for higher piezoelectric performance.[22] The high-speed rotating drum was utilized for preparing oriented microlines relative to the rotation direction.[23] Second, the obtained LCP/P(VDF-TrFE) fabrics were immersed in PEI (ethanol solution) for 6 h to complete the post-crosslinking process, and then dried in vacuum at 50 °C for 6 h. The oriented CLCP/P(VDF-TrFE) fabrics were formed on large scale (Figure 1e) with an average fiber diameter of ≈200 nm (Figure S2a, Supporting Information). Then, the CLCP/P(VDF-TrFE) fabrics were immersed in pure ILs for 12 h, and then dried in vacuum at room temperature for 6 h, to prepare ILCP/P(VDF-TrFE) fabrics. The fibers in ILCP/P(VDF-TrFE) were coalesced to form porous layers (Figure S2b, Supporting Information). The ILs used in this work are hydrophobic 1-ethyl-3-methylimidazolium bis-(trifluoromethylsulfonyl)imide ([EMIm][TFSI]), which exhibit high voltage stability, chemical and thermal stability, and humidity resistance.[24] The IL content in ILCP/P(VDF-TrFE) increased to 58% and the ionic conductivity reached 0.53 mS cm^{-1} after immersion for 12 h (Figure S3, Supporting Information), corresponding to internal resistance of ≈1 MΩ. Compared to the two electrodes of AgNWs and conductive fabrics, ILCP/P(VDF-TrFE) fabrics can be still considered as dielectric materials.[25] The polarizing optical microscopic

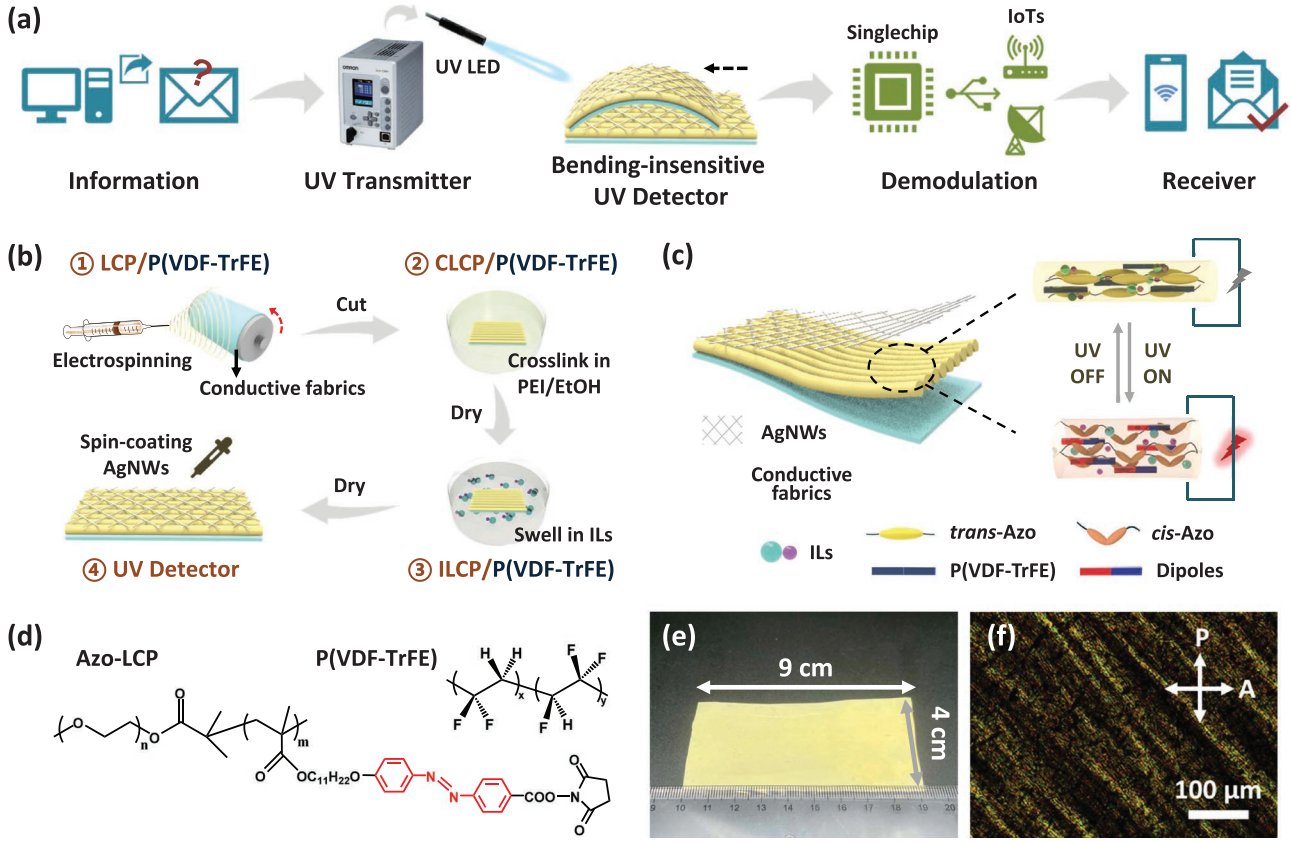

Figure 1. a) Schematic diagram of UV communication system based on the bending-insensitive UV detector. b) Schematic illustration of the fabrication process of the ILCP/P(VDF-TrFE) device. c) Schematic illustration of the composite structure and working mechanism for the ILCP/P(VDF-TrFE) device. d) Chemical structures of the Azo-LCP and P(VDF-TrFE) used in this study. e) The photograph of large-scale CLCP/P(VDF-TrFE) fabrics with a size of 9 cm × 4 cm × 30 μm. f) POM image of the texture of ILCP/P(VDF-TrFE) fibers at room temperature. P: polarizer, A: analyzer.

(POM) images determine the orientation of LC microlines on the whole due to electrostatic fields and high-speed rotation upon electrospinning (Figure 1f and Figure S4, Supporting Information). Finally, the piezoelectric UV detector was fabricated by spin-coating diluted silver nanowire (AgNW) suspension onto the ILCP/P(VDF-TrFE) fabrics (Figure S2c,d, Supporting Information). The spin-coated AgNWs exhibited an average sheet resistance of 54 Ω sq^{-1}, possessing high degree of uniformity (Figure S5, Supporting Information). The ILCP/P(VDF-TrFE) fabrics demonstrate the mechanical properties of 74% elongation and 7.7 MPa tensile strength (Figure S6, Supporting Information), benefiting from the enhancement of LC networks and plasticization of ILs, meeting the needs of wearable devices.[26]

2.2. Performance of the ILCP/P(VDF-TrFE) Device

The current response to UV illuminance of the ILCP/P(VDF-TrFE) device is presented in **Figure 2**a,b. The device exhibited an increased short-circuit current (I_{SC}) signal in response to UV light, with a dark current of ≈5 nA. The device can be seen as piezoelectric nanogenerators with tunable internal resistance via UV illumination. The experimentally measured current signal in this work is an AC/DC combined signal, which can be separated into ≈1 nA pulse-like AC signal by the piezoelectric effect, and ≈4 nA platform-like DC signal by resistive effect, under 0.2 mW cm^{-2} UV light. As shown in the fitting curves of separated AC and DC signals versus UV power density (Figure S7a, Supporting Information), the AC signal contributes to ≈20% of the ΔI_{SC} data. When the weight ratio of Azo-LCP/P(VDF-TrFE) was 1:3, the fitted relationship between I_{SC} changes and UV power density was calculated by linear regression method. The slope of the fitting curve stands for the responsivity (R) of the ILCP/P(VDF-TrFE) device, defined as the following equations.

$$\Delta I_{SC} = 23.5 \times P + 0.20 \quad (1)$$

$$R = \Delta I_{SC} / PS \quad (2)$$

where ΔI_{SC} is the short-circuit current change, P represents the UV power density, and S is the effective area under irradiation.

The corresponding open-circuit voltage (V_{OC}) is recorded in Figure S8 (Supporting Information). Upon 1.0 mW cm^{-2} UV illuminance (365 nm), the ILCP/P(VDF-TrFE) device with an area size of 20 × 10 mm^2 can generate a V_{OC} of 0.29 mV and a ΔI_{SC} of 24 nA. The device demonstrated a response time of 190 ms, a recovery time of 200 ms (Figure S7b, Supporting Information), a responsivity of 11.8 μA W^{-1} at zero bias, an

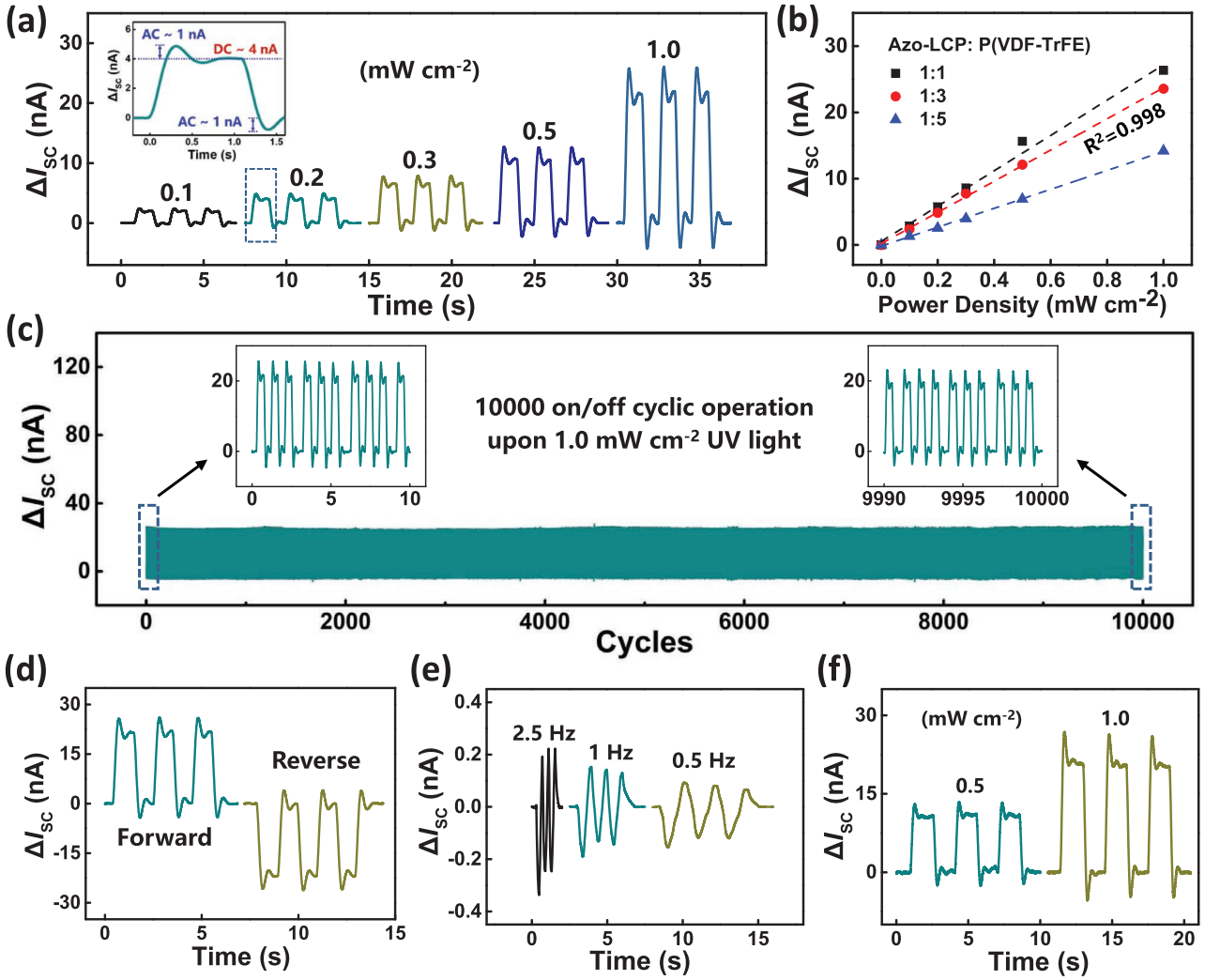

Figure 2. a) Experimentally measured short-circuit current (*I*sc) changes in accordance with UV power density from 0.1 to 1.0 mW cm^{-2}. The inset shows the response signal is an AC/DC combined signal. The weight ratio of Azo-LCP/P(VDF-TrFE) is 1:3. b) Experimental data and fitting curves of *I*sc changes versus UV power density in different Azo-LCP/P(VDF-TrFE) weight ratios. c) Device response during consecutive 10 000 UV on/off cyclic operation upon 1.0 mW cm^{-2} UV light. The insets are the initial (left) and last (right) ten cycles of the test. d) Results of the switching polarity test (forward and reverse connections) under 1.0 mW cm^{-2} UV light. The weight ratio of Azo-LCP/P(VDF-TrFE) is 1:3. e) Experimentally measured I_{SC} changes from the ILCP/P(VDF-TrFE) device during dynamic bending with 200 m^{-1} curvatures in different frequency. f) Experimentally measured I_{SC} changes in accordance with UV power density of 0.5 and 1.0 mW cm^{-2}, under a dynamic bending frequency of 2.5 Hz with 200 m^{-1} curvatures.

illuminance resolution of 0.1 mW cm^{-2}, and a linear correlation coefficient of 0.998, which is significantly improved compared with our reported work (response time of 5 s, recovery time of 4 s, and illuminance resolution of 5 mW cm^{-2}).[16] With the decrease of Azo-LCP content, the responsivity of the device is reduced because of the smaller contraction stress. When the weight ratio of Azo-LCP/P(VDF-TrFE) increased to 1:1, the responsivity increased slightly due to the large molar extinction coefficient of azobenzene and thus short optical path length in the thickness direction of films.[12b] Although high-content CLCPs produce large contraction stress, the UV irradiation only arrives at the surface region of the ILCP/P(VDF-TrFE) device, leading to the limited increase of the responsivity.

Upon 1.0 mW cm^{-2} UV light, the ΔI_{SC} was constantly stable in the static test, undergoing 10 000 on/off testing cycles and 200 m^{-1} bending curvature (Figure 2c and Figure S9, Supporting Information). The device performance almost remained unchanged after consecutive 2000 cycles of folding operation, profiting from the robustness of ILCP/P(VDF-TrFE) (Figure S10, Supporting Information). It is suggesting that the samples have no obvious cracks on the surface and cross-section morphologies after 2000 folding cycles (Figure S11, Supporting Information). The device also exhibited waterproof stability upon 100 wetting cycles in water because of the humidity resistance of the whole system (Figure S9c, Supporting Information). The comprehensive performance, such as flexibility and response time, of the ILCP/P(VDF-TrFE) device is comparable with reported self-powered wearable UV detectors (Table S1, Supporting Information). The response time of the ILCP/P(VDF-TrFE) device is nearly two orders of magnitude faster than reported wearable functional polymer-based UV detectors.[9] The response time and responsivity

almost reach the same order of magnitude as reported in wearable semiconductor-based UV detectors, such as TiO_2/P3HT.[27] Nevertheless, the flexibility of ILCP/P(VDF-TrFE) device far exceeds that of semiconductor device.

The switching polarity test of ILCP/P(VDF-TrFE) device was shown in Figure 2d. The ΔIsc data in forward and reverse connections exhibit opposite polarity with almost identical amplitude, which demonstrates the measured electrical signals indeed originated from piezoelectric output. Especially, the device demonstrated a ΔI_{SC} of ≈0.2 nA during dynamic bending frequency of 2.5 Hz with 200 m^{-1} curvatures without UV illuminance, due to the significant intrinsic flexibility and compatibility of composite fabrics (Figure 2e and Movie S1, Supporting Information). Therefore, it can be concluded that the device exhibits a bending insensitivity of less than 1% performance variation under 1.0 mW cm^{-2} UV light (Figure 2f), extending the practical applications of the device under dynamic bending state.

2.3. Working Mechanism of the ILCP/P(VDF-TrFE) Device

To investigate the working mechanism of the ILCP/P(VDF-TrFE) device, X-ray diffraction (XRD) and Fourier transform infrared spectroscopy (FT-IR) were carried out to characterize the crystalline structure of the ILCP/P(VDF-TrFE) fabrics (**Figure 3**a,b). The electrospun P(VDF-TrFE) and ILCP/P(VDF-TrFE) fabrics showed the dominant diffraction peaks at 20.6° in XRD patterns, and characteristic bands at 840 and 1280 cm^{-1} in FT-IR spectra, assigned to the β-phase crystalline structure.[28] In XRD patterns, the peaks of α-phase and γ-phase reduced in intensity for electrospun fabrics. According to FT-IR spectra, the calculated β-phase contents of P(VDF-TrFE) powders, P(VDF-TrFE) fabrics, and ILCP/P(VDF-TrFE) fabrics were 36.7%, 84.9%, and 71.9%, respectively (Table S2, Supporting Information). From XRD and FT-IR results, it can be concluded that a more β-phase crystalline structure is formed during the electrospinning. In this fabrication procedure, the P(VDF-TrFE) copolymers are subjected to high-ratio stretching and electric poling upon electrospinning, leading to effective crystallization of β-phase PVDF. Thus, it is not so necessary to treat P(VDF-TrFE) copolymers with other approaches, such as drawing, annealing, etc.[29]

The crystallinity of P(VDF-TrFE) was further analyzed by DSC data (Figure S12, Supporting Information). The calculated crystallinity of P(VDF-TrFE) powders, P(VDF-TrFE) fabrics, and LCP/P(VDF-TrFE) fabrics were 41.4%, 53.8%, and 54.2%, respectively (Table S2, Supporting Information). To further confirm the molecular compatibility between LCPs and P(VDF-TrFE), dynamic mechanical analysis (DMA) was conducted to demonstrate the glass transition temperature (T_g) of LCP/P(VDF-TrFE) fabrics (Figure S13, Supporting Information). In the case of semicrystalline P(VDF-TrFE), two T_g are usually observed. One at ≈-30 °C attributes to segmental motions in the amorphous region and the other one at ≈90 °C relates to segmental motions in the crystalline region. The T_g of Azo-LCPs is ≈75 °C.[16] Thus, the LCP/P(VDF-TrFE) fabrics have the fused and higher T_g peak at ≈90 °C compared to pure P(VDF-TrFE) fabrics, confirming the compatibility between LCPs and P(VDF-TrFE). In this work, the ILCP/P(VDF-TrFE) fabrics containing 33.3 wt.% LCPs still maintain a high β-phase content, because of the great molecular compatibility between LCPs and P(VDF-TrFE).

To further illustrate the microscopic deformation of ILCP/P(VDF-TrFE) fabrics, in situ characterizations of POM images of the microlines before and after UV irradiation are presented in Figure 3c,d and Movie S2 (Supporting Information). Because of the contraction stress from Azo-CLCPs upon UV light, the microlines deformed microscopically and the alignment of mesogens was changed. It is reasonable that the contraction stress and microscopic deformation drive the movement of P(VDF-TrFE) dipoles to output forward AC piezoelectric signals spontaneously. When turning off UV light, the contraction stress is immediately released because of the high Young's modulus of P(VDF-TrFE), generating reverse AC piezoelectric signals. To demonstrate the significance of microstructures in the device, the ILCP/P(VDF-TrFE) film with the 1:3 weight ratio of Azo-LCP/P(VDF-TrFE) was obtained by casting electrospinning solution on a PTFE mold and then drying at 50 °C in vacuum, possessing the same thickness of ≈30 μm with fabrics. The ILCP/P(VDF-TrFE) casting film exhibited too poor sensitivity (Figure S14, Supporting Information), compared to ILCP/P(VDF-TrFE) fabrics (Figure 2a).

In addition, the oriented microline structure of ILCP/P(VDF-TrFE) fabrics clearly enhanced the UV-induced contraction stress (Figure S15, Supporting Information), because of the improved anisotropy of mesogens and alignment of dipoles, resulting in higher responsive currents to UV light. The introduction of ILs also significantly facilitates the high sensitivity of the device due to the synergistic effect of resistive and piezoelectric effects (Figure S16, Supporting Information). The UV light-triggered contraction stress from Azo-CLCPs effectively transfers to ILs through the P(VDF-TrFE) matrix and then accelerates the ion migration, amplifying electric signals rapidly, which are DC-like signals. To further confirm the synergistic effect of piezoelectric and resistive effects, highly elastic polyurethane (TPU) was incorporated into the ILCP/P(VDF-TrFE) fabrics (Figure S17, Supporting Information). With the increase of TPU content, the current signals obviously decreased and the response time became slower because the viscoelasticity of TPU restrains the stress transmission to P(VDF-TrFE) and then suppresses the piezoelectric effects. Therefore, the combination of Azo-CLCPs, ILs, and P(VDF-TrFE) establishes an effective conversion mechanism of UV illuminance-internal stress-current signals by coupling resistive and piezoelectric effects, which endows high sensitivity for the wearable devices.

On the other hand, it is reported that mechanical drawing of the Azo-CLCPs can induce the *cis*-to-*trans* isomerization of azobenzene and align the mesogens along the stretching direction.[30] Herein, the recovery stress and transient piezopotential of P(VDF-TrFE) can facilitate the re-alignment of CLCPs upon turning off UV light. As shown in the UV–vis absorption spectra of ILCP/P(VDF-TrFE) fabrics before and after UV irradiation (Figure 3e–h), the peak intensity at 360 nm is corresponding to the π–π^* transition of the *trans*-azobenzene.[31] The *trans*-Azo content is defined as the ratio of absorption intensity over the pristine absorption intensity at 360 nm. Upon UV irradiation, the *trans*-Azo content decreased to 99.1 mol% at 0.2 s and then leveled off to a platform of 95.4 mol% for 20 s. Then, the

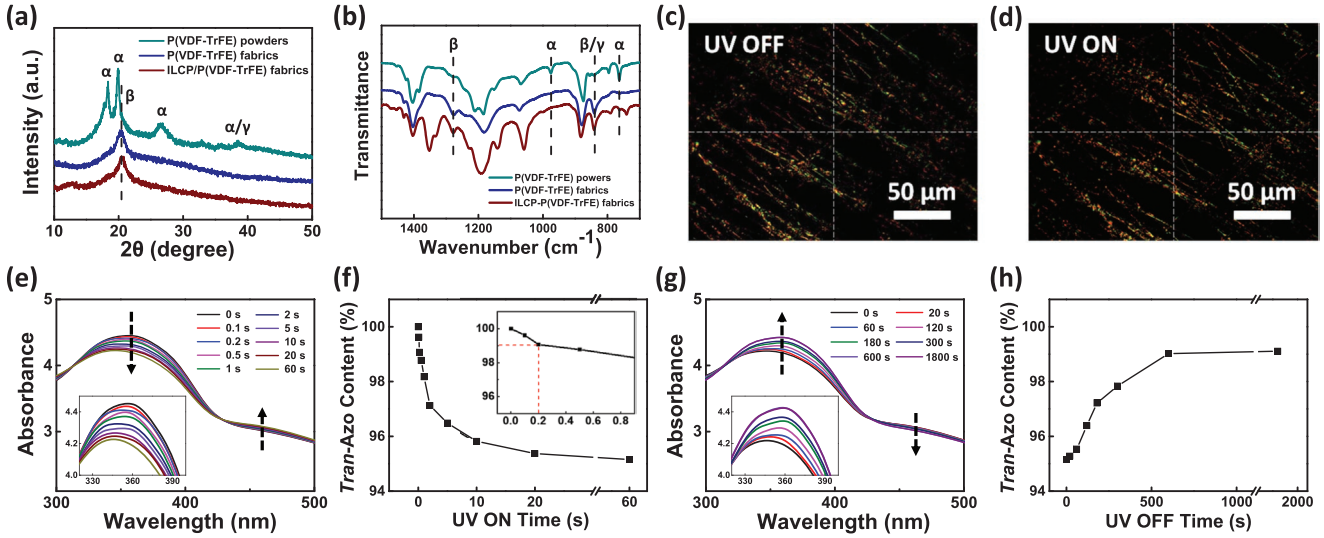

Figure 3. a) XRD patterns and b) FT-IR spectra of P(VDF-TrFE) powders, P(VDF-TrFE) fabrics, and ILCP/P(VDF-TrFE) fabrics. c,d) POM images of the texture of the ILCP/P(VDF-TrFE) fibers before and after UV irradiation. The dotted lines stand for crossed polarizer, assisted to recognize the deformation of fibers. UV–vis absorption spectra and curves of *trans*-Azo content versus time in the ILCP/P(VDF-TrFE) fabrics upon e,f) turning on UV irradiation (10 mW cm^{-2}), and g,h) turning off UV irradiation, respectively. The *trans*-Azo content is defined as the ratio of absorption intensity over the pristine absorption intensity at 360 nm. Film thickness: 5 μm.

trans-Azo content recovered to 99.0 mol% upon turning off UV light for 10 min. The absorption intensity decreased and recovered completely in the subsequent cycles under alternative UV on/off operation (Figure S18, Supporting Information). It is suggesting that the *cis*-Azo in fabrics can switch to *trans*-Azo spontaneously upon turning off the UV light, bringing in a fast cyclic operation of the device in the absence of visible light or heating.

2.4. Applications of Bending-Insensitive UV Communication System

As discussed above, it is obvious that dynamic bending motions of the ILCP/P(VDF-TrFE) device have little effect on the UV sensing signals. Because the wearable military equipment is inevitably subject to dynamic bending, the bending-insensitive UV detector is highly desirable for UV communication system in the military field. In addition, the electric signal output of the device allows it for the facile integration into the IoTs system. Taking advantage of the high responsivity and ultrafast response speed, we have designed the wearable and bending-insensitive UV communication system based on ILCP/P(VDF-TrFE) fabrics (**Figure 4** and Figure S19, Supporting Information).

The input information was encrypted by ASCII, which is a common computer character encoding with 8-bit binary characters. ASCII reserves 256 characters in total, including control characters (such as carriage return and backspace), and printable characters (alphabets, numbers, and symbols) on a keyboard. After signal conversion, the information was sent by a program-controlled UV transmitter. The "0" and "1" codes in the 8-bit binary character encoding were represented by the UV illuminance signals, such as 5 and 10 mW cm^{-2}, respectively, which can avoid the interference from solar UV radiation.[32] The UV signals were wirelessly transmitted in free space and recognized by the ILCP/P(VDF-TrFE) device. In the static test, the current signals exhibit a sequence of low-level and high-level signals, standing for the "0" and "1" codes for the subsequent demodulation (Figure 4a and Movie S3, Supporting Information). For instance, the ASCII encoding of the letter "A" is corresponding to 8-bit binary characters of "0 100 0001". After decoding the "0" and "1" sequences by the IoTs system, the information was recognized and transferred to a remote smartphone receiver through Bluetooth, resulting in the output of "A" on the screen. It is notable that the printing speed is 3.2 s per character, much faster than our previous work.[16]

Particularly, the device also guarantees stable UV communication in the dynamic bending test even under a bending frequency of 2.5 Hz with 200 m^{-1} curvatures (Figure 4b–d and Movie S3, Supporting Information), which is much higher than the bending frequency of human activity. The current signals of the letter "A" under the dynamic bending test are almost the same as the signals under static test. Similarly, the number "1" and symbol "@" were recognized and outputted on the smartphone receiver. The information can be re-encrypted and transformed by simply modulating the ASCII encoding. The wearable UV communication system is also successfully implemented on a human wrist under a bending frequency of ≈1 Hz (Figure S20 and Movie S4, Supporting Information). Moreover, the self-powered ILCP/P(VDF-TrFE) fabrics not only facilitate the performance of detector, but also enhance the sustainability and independence of the UV communication system. Since UV light is a cold light source, the device produces little heat upon working, which avoids being intercepted and interfered with. The device demonstrates stable UV communication performance under dynamic bending test for the first time, featuring portability, low energy consumption, high speed, and anti-electromagnetic interference.

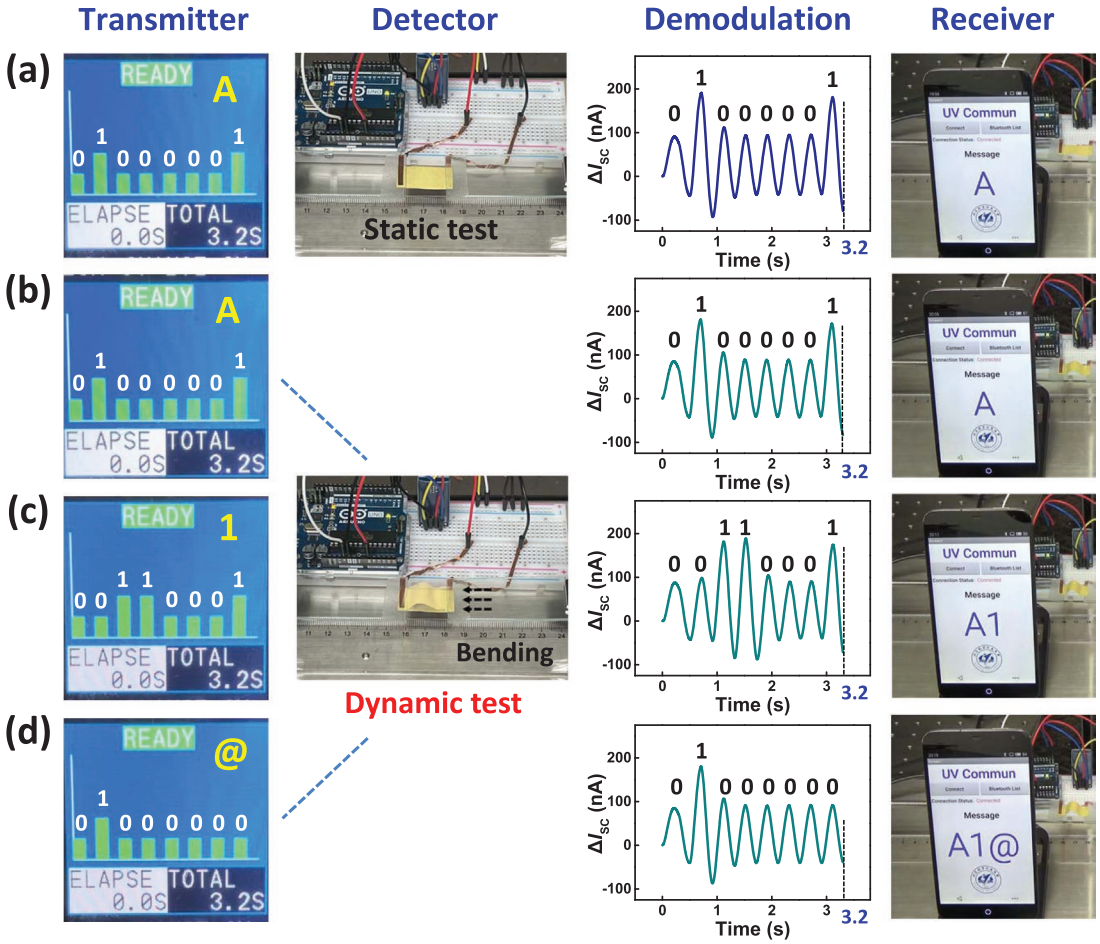

Figure 4. Photographs of the practical working process of UV communication system under a) static test and b–d) dynamic bending test, containing the encoding of UV transmitter by ASCII, corresponding 8-bit binary characters, demodulation of measured current signals, and the decoding results in remote smartphone receiver, respectively. The device was fixed on a linear motor under a bending frequency of 2.5 Hz with 200 m^{-1} curvatures. The codes of "0" and "1" in the UV transmitter are set as 5 and 10 mW cm^{-2} UV light, respectively. The ASCII encoding of "A", "1", and "@" are corresponding to 8-bit binary characters of "0 100 0001", "001 10001", and "0 100 0000", respectively.

3. Conclusion

In summary, we report a bending-insensitive and self-powered UV detector based on the electrospun composite fabrics with oriented microlines, consisting of UV responsive Azo-CLCPs, hydrophobic ILs, and piezoelectric P(VDF-TrFE) nanogenerators. The conversion mechanism of UV illuminance-mechanical stress-electric signals by coupling resistive and piezoelectric effects significantly facilitates the performance of full polymer-based UV detectors. The ILCP/P(VDF-TrFE) device exhibits fast response time of 190 ms, recovery time of 200 ms, responsivity of 11.8 μA W^{-1} at zero bias, and an illuminance resolution of 0.1 mW cm^{-2}. In addition, the high Young's modulus and piezopotential of P(VDF-TrFE) accelerate the *cis*-to-*trans* isomerization of Azo-CLCPs in the absence of visible light or heating, contributing to the fast UV on/off cyclic operation of the device. The ILCP/P(VDF-TrFE) device demonstrates a bending insensitivity of less than 1% performance variation (1.0 mW cm^{-2} UV light) under bending frequency of 2.5 Hz with 200 m^{-1} curvatures, benefiting from the intrinsic flexibility of the whole composite system. The device maintains stable performance upon 10 000 UV on/off testing cycles and 100 wetting cycles in water. Furthermore, wearable information encoding and encryption devices based on ILCP/P(VDF-TrFE) fabrics are successfully developed for bending-insensitive UV communication system via the IoTs technologies. The capability of data communication from UV transmitter to remote smartphone receiver has been well demonstrated with a printing speed of 3.2 s per character by ASCII encoding, especially under the dynamic bending state. The bending-insensitive and self-powered device with ultrafast response speed provides a generalizable approach for the optimization of smart polymer-based wearable electronics, extending practical applications under various extreme and special environments.

4. Experimental Section

Materials: Branched polyethyleneimine (PEI, M_w = 1 × 10^4 g mol^{-1}, 99%, Aladdin), poly(vinylidene fluoride-trifluoroethylene) (P(VDF-TrFE), 70: 30, Solvay), and 1-ethyl-3-methylimidazolium

bis-(trifluoromethylsulfonyl)imide ([EMIm][TFSI], 99%, Adamas), Acetone (99.5%, Adamas), N, N-dimethylformamide (DMF, 99.9%, Aladdin), Ethanol (EtOH, 99.8%, Aladdin), silver nanowires (AgNWs, 1 wt.% aqueous dispersion, diameter ≈25 nm, length ≈17 µm, Beijing Hi-nano Technology), conductive fabrics (single-sided adhesive tapes, polyester fabrics with copper fibers, with a sheet resistance of 35 mΩ sq^{-1} and a thickness of 100 µm, Shenzhen Huijia) were used as received. The Azo-LCPs (PEO_{45}-*b*-$PMA(Az)_{28}$, $M_n = 1.82 \times 10^4$ g mol^{-1}, $M_w/M_n = 1.13$), were synthesized by atom transfer radical polymerization (ATRP).[33]

Fabrication of the UV Detector: First, the 5 wt.% Azo-LCPs and 15 wt.% P(VDF-TrFE) solution was prepared by dissolving Azo-LCPs and P(VDF-TrFE) powders in DMF and acetone mixture (volume ratio 6:4) through stirring at room temperature for 12 h. The homogeneous solution was transferred into a plastic syringe with a 21-gauge metallic nozzle. An electrospinning device (Ucalery, ET-2535X) was used to produce fibers with a positive voltage of 15 kV and a feed rate of 1 mL h^{-1}. The distance between the metallic nozzle and cylinder was set at 12 cm. A rotating cylinder wrapped in conductive fabrics rotated at a uniform speed of 2800 rpm as a collector to obtain oriented fibers. The LCP/P(VDF-TrFE) fabrics were immersed in an ethanol solution of PEI (2 mg mL^{-1}) for 6 h and then dried in vacuum overnight. Subsequently, the obtained CLCP/P(VDF-TrFE) fabrics were swollen in pure ILs for 12 h and then dried in vacuum at room temperature overnight. The free-standing ILCP/P(VDF-TrFE) fabrics were finally obtained. The AgNW suspension was diluted by ethanol to the concentration of ≈3 mg mL^{-1}, and homogenized by ultrasonic vibration for 3 min. The diluted AgNW suspension was deposited twice on the ILCP/P(VDF-TrFE) fabrics (20×10 mm^2), using a spin coater at 2000 rpm for 60 s. Before the electrical measurements, copper wires were attached to the opposite sides of the UV detector by silver paste.

Characterization and Measurements: The morphology of ILCP/P(VDF-TrFE) fabrics was observed using a scanning electron microscope (TESCAN VEGA3). The crystalline structures of P(VDF-TrFE) and ILCP/P(VDF-TrFE) were determined by the measurements of X-ray diffraction (Bruker D8 Advance) and Fourier transform infrared spectroscopy (Nicolet 6700). UV–vis spectra of the ILCP/P(VDF-TrFE) fabrics were recorded on a Shimadzu UV-2600 spectrophotometer. Textures of the ILCP/P(VDF-TrFE) fabrics were observed on a polarizing optical microscope (POM, Shangguang 59XF). The conductivity and sheet resistance were measured by a four-point probe meter (ST2253, Suzhou Jingge Electronic Co., LTD). The dynamic mechanical analysis was carried out by a mechanical analyzer (TA Instruments, Waters Ltd., DMA 850). UV light (365 nm) was obtained from Omron (ZUV-C30H) LED irradiator. Visible light (520 nm) was obtained from CCS (HLV-22GR-3W) LED irradiator. The current response was measured by an electrometer (Keithley 6517B). The tensile properties were measured in a stretch mode at a strain rate of 3 mm min^{-1} at room temperature on a mechanical analyzer (Xieqiang CTM2050). The Android application for UV communication was designed by MIT App Inventor 2. All the photos and movies were recorded on a SONY HDR-CX450 digital video camera.

Statistical Analysis: The short-circuit current (*Isc*) changes were averaged from three individual measurements. The data were directly obtained from an electrometer (Keithley 6517B). All the analyses were performed using Origin Pro 9.0 software.

Supporting Information

Supporting Information is available from the Wiley Online Library or from the author.

Acknowledgements

This work was financially supported by the National Natural Science Foundation of China (No. 52173193), the Natural Science Foundation of Beijing Municipality (No. 2202024), and the Equipment Pre-research Foundation of China's Central Military Commission (No. 80922010501).

Conflict of Interest

The authors declare no conflict of interest.

Data Availability Statement

The data that support the findings of this study are available from the corresponding author upon reasonable request.

Keywords

bending-insensitive UV detectors, liquid crystalline polymers, nanogenerators, self-powered wearable UV detectors, UV detectors

Received: April 28, 2022
Revised: July 6, 2022
Published online:

[1] a) E. Song, J. Li, S. M. Won, W. Bai, J. A. Rogers, *Nat. Mater.* **2020**, *19*, 590; b) G.-H. Lee, H. Moon, H. Kim, G. H. Lee, W. Kwon, S. Yoo, D. Myung, S. H. Yun, Z. Bao, S. K. Hahn, *Nat. Rev. Mater.* **2020**, *5*, 149; c) X. Wang, L. Dong, H. Zhang, R. Yu, C. Pan, Z. L. Wang, *Adv. Sci.* **2015**, *2*, 1500169; d) J. C. Yang, J. Mun, S. Y. Kwon, S. Park, Z. Bao, S. Park, *Adv. Mater.* **2019**, *31*, 1904765.

[2] a) S. Premi, S. Wallisch, C. M. Mano, A. B. Weiner, A. Bacchiocchi, K. Wakamatsu, E. J. H. Bechara, R. Halaban, T. Douki, D. E. Brash, *Science* **2015**, *347*, 842; b) Y. Zou, Y. Zhang, Y. Hu, H. Gu, *Sensors* **2018**, *18*, 2072; c) H. Chen, K. Liu, L. Hu, A. A. Al-Ghamdi, X. Fang, *Mater. Today* **2015**, *18*, 493; d) S. Chen, Z. Lou, D. Chen, G. Shen, *Adv. Mater.* **2018**, *30*, 1705400.

[3] D. Han, Y. Liu, K. Zhang, P. Luo, M. Zhang, *Opt. Express* **2012**, *20*, 15833.

[4] S. Cai, X. Xu, W. Yang, J. Chen, X. Fang, *Adv. Mater.* **2019**, *31*, 1808138.

[5] a) Y.-Q. Zheng, Y. Liu, D. Zhong, S. Nikzad, S. Liu, Z. Yu, D. Liu, H.-C. Wu, C. Zhu, J. Li, H. Tran, J. B.-H. Tok, Z. Bao, *Science* **2021**, *373*, 88; b) A. Romeo, Q. Liu, Z. Suo, S. P. Lacour, *Appl. Phys. Lett.* **2013**, *102*, 131904.

[6] a) X. Liu, L. Gu, Q. Zhang, J. Wu, Y. Long, Z. Fan, *Nat. Commun.* **2014**, *5*, 4007; b) S. H. Park, R. Su, J. Jeong, S.-Z. Guo, K. Qiu, D. Joung, F. Meng, M. C. McAlpine, *Adv. Mater.* **2018**, *30*, 1803980.

[7] a) W. Wang, S. Wang, R. Rastak, Y. Ochiai, S. Niu, Y. Jiang, P. K. Arunachala, Y. Zheng, J. Xu, N. Matsuhisa, X. Yan, S.-K. Kwon, M. Miyakawa, Z. Zhang, R. Ning, A. M. Foudeh, Y. Yun, C. Linder, J. B.-H. Tok, Z. Bao, *Nat. Electron.* **2021**, *4*, 143; b) H. Tran, V. R. Feig, K. Liu, Y. Zheng, Z. Bao, *Macromolecules* **2019**, *52*, 3965; c) S. Wang, J. Xu, W. Wang, G.-J. N. Wang, R. Rastak, F. Molina-Lopez, J. W. Chung, S. Niu, V. R. Feig, J. Lopez, T. Lei, S.-K. Kwon, Y. Kim, A. M. Foudeh, A. Ehrlich, A. Gasperini, Y. Yun, B. Murmann, J. B.-H. Tok, Z. Bao, *Nature* **2018**, *555*, 83.

[8] a) W. Feng, D. J. Broer, D. Q. Liu, *Adv. Funct. Mater.* **2020**, *30*, 7; b) H. Finkelmann, E. Nishikawa, G. G. Pereira, M. Warner, *Phys. Rev. Lett.* **2001**, *87*, 4.

[9] a) H. Nie, N. S. Schauser, N. D. Dolinski, J. Hu, C. J. Hawker, R. A. Segalman, J. Read de Alaniz, *Angew. Chem., Int. Ed.* **2020**, *59*, 5123; b) P. Li, S. Tan, Y. Wu, C. Wang, M. Watanabe, *ACS Macro Lett.* **2020**, *9*, 825; c) H. Wang, C. N. Zhu, H. Zeng, X. Ji, T. Xie, X. Yan, Z. L. Wu, F. Huang, *Adv. Mater.* **2019**, *31*, 1807328.

[10] a) T. J. White, D. J. Broer, *Nat. Mater.* **2015**, *14*, 1087; b) Y. Yu, M. Nakano, T. Ikeda, *Nature* **2003**, *425*, 145; c) T. H. Ware, M. E. McConney, J. J. Wie, V. P. Tondiglia, T. J. White, *Science* **2015**,

347, 982; d) A. H. Gelebart, D. J. Mulder, M. Varga, A. Konya, G. Vantomme, E. W. Meijer, R. L. B. Selinger, D. J. Broer, *Nature* **2017**, *546*, 632.

[11] A. Kotikian, J. M. Morales, A. Lu, J. Mueller, Z. S. Davidson, J. W. Boley, J. A. Lewis, *Adv. Mater.* **2021**, *33*, 2101814.

[12] a) C. Zhu, Y. Lu, L. Jiang, Y. Yu, *Adv. Funct. Mater.* **2021**, *31*, 2009835; b) X. Pang, J.-a. Lv, C. Zhu, L. Qin, Y. Yu, *Adv. Mater.* **2019**, *31*, 1904224; c) Z.-C. Jiang, Y.-Y. Xiao, L. Yin, L. Han, Y. Zhao, *Angew. Chem., Int. Ed.* **2020**, *59*, 4925.

[13] a) X. Lu, H. Zhang, G. Fei, B. Yu, X. Tong, H. Xia, Y. Zhao, *Adv. Mater.* **2018**, *30*, 1706597; b) A. Kotikian, R. L. Truby, J. W. Boley, T. J. White, J. A. Lewis, *Adv. Mater.* **2018**, *30*, 1706164.

[14] S. R. A. Ruth, V. R. Feig, H. Tran, Z. Bao, *Adv. Funct. Mater.* **2020**, *30*, 2003491.

[15] S. R. A. Ruth, L. Beker, H. Tran, V. R. Feig, N. Matsuhisa, Z. A. Bao, *Adv. Funct. Mater.* **2020**, *30*, 1903100.

[16] X. Zheng, Y. Jia, A. Chen, *Nat. Commun.* **2021**, *12*, 4875.

[17] Q. Sun, D. H. Kim, S. S. Park, N. Y. Lee, Y. Zhang, J. H. Lee, K. Cho, J. H. Cho, *Adv. Mater.* **2014**, *26*, 4735.

[18] a) L. Su, H. Y. Li, Y. Wang, S. Y. Kuang, Z. L. Wang, G. Zhu, *Nano Energy* **2017**, *31*, 264; b) Y. Zhang, M. Peng, Y. Liu, T. Zhang, Q. Zhu, H. Lei, S. Liu, Y. Tao, L. Li, Z. Wen, X. Sun, *ACS Appl. Mater. Interfaces* **2020**, *12*, 19384.

[19] a) A. Chen, C. Zhang, G. Zhu, Z. L. Wang, *Adv. Sci.* **2020**, *7*, 2000186; b) A. Wang, Z. Liu, M. Hu, C. Wang, X. Zhang, B. Shi, Y. Fan, Y. Cui, Z. Li, K. Ren, *Nano Energy* **2018**, *43*, 63; c) B. Azimi, M. Milazzo, A. Lazzeri, S. Berrettini, M. J. Uddin, Z. Qin, M. J. Buehler, S. Danti, *Adv. Healthcare Mater.* **2020**, *9*, 1901287.

[20] Y. Wan, Y. Wang, C. F. Guo, *Mater. Today Phys.* **2017**, *1*, 61.

[21] a) K. Dong, X. Peng, Z. L. Wang, *Adv. Mater.* **2020**, *32*, 1902549; b) S. B. Kang, S. H. Won, M. J. Im, C. U. Kim, W. I. Park, J. M. Baik, K. J. Choi, *Nanotechnology* **2017**, *28*, 11.

[22] R. K. Zheng, Y. Yang, Y. Wang, J. Wang, H. L. W. Chan, C. L. Choy, C. G. Jin, X. G. Li, *Chem. Commun.* **2005**, https://doi.org/10.1039/b417033d1447.

[23] S. F. Fennessey, R. J. Farris, *Polymer* **2004**, *45*, 4217.

[24] a) Y. M. Kim, H. C. Moon, *Adv. Funct. Mater.* **2020**, *30*, 1907290; b) S. Zhang, Q. Zhang, Y. Zhang, Z. Chen, M. Watanabe, Y. Deng, *Prog. Mater. Sci.* **2016**, *77*, 80.

[25] S. Yu, Y. Zhang, Z. Yu, J. Zheng, Y. Wang, H. Zhou, *Nano Energy* **2021**, *80*, 105519.

[26] A. Chortos, J. Liu, Z. Bao, *Nat. Mater.* **2016**, *15*, 937.

[27] a) L. Zheng, X. Deng, Y. Wang, J. Chen, X. Fang, L. Wang, X. Shi, H. Zheng, *Adv. Funct. Mater.* **2020**, *30*, 2001604; b) Z. Zhu, Y. Gu, S. Wang, Y. Zou, H. Zeng, *Adv. Electron. Mater.* **2017**, *3*, 1700281.

[28] a) B. H. Moghadam, M. Hasanzadeh, A. Simchi, *ACS Appl. Nano Mater.* **2020**, *3*, 8742; b) A. Gheibi, R. Bagherzadeh, A. A. Merati, M. Latifi, *J. Polym. Res.* **2014**, *21*, 14; c) C. K. Jeong, D. Y. Hyeon, G.-T. Hwang, G.-J. Lee, M.-K. Lee, J.-J. Park, K.-I. Park, *J. Mater. Chem. A* **2019**, *7*, 25481; d) Y. Liu, H. Aziguli, B. Zhang, W. Xu, W. Lu, J. Bernholc, Q. Wang, *Nature* **2018**, *562*, 96; e) Aaryashree, S. Sahoo, P. Walke, S. K. Nayak, C. S. Rout, D. J. Late, *Nano Res.* **2021**, *14*, 3669; f) S. Kalani, R. Kohandani, R. Bagherzadeh, *RSC Adv.* **2020**, *10*, 35090; g) G. Zandesh, A. Gheibi, M. S. S. Bafqi, R. Bagherzadeh, M. Ghoorchian, M. Latifi, *J. Ind. Text.* **2017**, *47*, 348.

[29] a) G. Ren, F. Cai, B. Li, J. Zheng, C. Xu, *Macromol. Mater. Eng.* **2013**, *298*, 541; b) A. Gheibi, M. Latifi, A. A. Merati, R. Bagherzadeh, *J. Polym. Res.* **2014**, *21*, 7.

[30] a) E.-h. Cho, K. Luu, S.-y. Park, *Macromolecules* **2021**, *54*, 5397; b) R. Bai, K. Bhattacharya, *J. Mech. Phys. Solids* **2020**, *144*, 104115.

[31] S. Guan, Z. Deng, T. Huang, W. Wen, Y. Zhao, A. Chen, *ACS Macro Lett.* **2019**, *8*, 460.

[32] L. Wang, W. Gong, Y. Ma, B. Hu, W. Wang, M. Zhang, *Energy* **2013**, *59*, 764.

[33] a) X. Zheng, S. Guan, C. Zhang, T. Qu, W. Wen, Y. Zhao, A. Chen, *Small* **2019**, *15*, 1900110; b) X. Zheng, Y. Zhao, A. Chen, *Polym. J. (Tokyo, Jpn.)* **2018**, *50*, 671; c) X. Zheng, Z. Li, Y. Zhao, T. Qu, S. Cao, P. Wang, Y. Li, T. Iyoda, A. Chen, *RSC Adv.* **2016**, *6*, 93298.